

DIRECT OBSERVATION OF THE FATE OF OCEANIC CARBON DIOXIDE RELEASE AT 800M

Edward T. Peltzer, Peter G. Brewer,
Gernot Friederich and Gregor Rehder
Monterey Bay Aquarium Research Institute
Moss Landing, CA 95039

Keywords: bubbles, carbon dioxide, clathrate hydrate, ocean sequestration

ABSTRACT

The rise rate and dissolution rate of freely released CO₂ in the ocean were measured to provide fundamental data regarding carbon sequestration in the upper ocean. These experimental observations were accomplished using MBARIs advanced remotely operated vehicle (ROV) technology. Small amounts of liquid CO₂ were released at 800 m depth and ambient temperature (4.4°C). The rising droplets were contained within an open ended acrylic chamber and were imaged with an HDTV camera. The mean rise rate for a droplet of initially 1 cm diameter observed over a one hour period was 12.4 cm/sec. The rise rate was initially about 10 cm/sec and it gradually increased to about 15 cm/sec as the bubble rose. The mean dissolution rate was 3.7 μmol/cm²/sec. Visual contact of the rising droplets was maintained for up to 1 hour and over 400 m initially suggesting a slow dissolution rate and long bubble lifetimes. However, 90% of the mass loss occurred within 30 minutes and 200 m of the release point.

INTRODUCTION

Concern about the rising levels of atmospheric CO₂ and the continued use of fossil fuels to meet ever increasing energy demands lead to consideration of the disposal of fossil fuel CO₂ in the ocean as a means of ameliorating greenhouse gas induced climate change (1,2). While many models of this process have been formulated (3,4), and various laboratory simulations have been carried out (5), there have been few direct oceanic experiments reported. With the availability of advanced ROV technology at MBARI, it was thought possible to carry out a controlled release of liquid and gaseous CO₂ in the open ocean, and to observe the processes taking place. In earlier work (6) we reported on contained experiments involving CH₄ and CO₂ to form hydrates. Here we present an initial experiment addressing the more difficult problem of observing and accurately measuring the behavior of a rising stream of freely released liquid CO₂. We choose this approach in order to evaluate the effectiveness of intermediate depth releases when all the co-varying properties of salinity, temperature, and pressure are present, and to represent the fluid dynamics of a rising cloud of liquid CO₂ droplets in the ocean.

In order to properly evaluate whether it is wise to proceed with any ocean disposal option, an accurate description of the fate of CO₂ injected into ocean water is necessary. At shallow depths (above about 350 m, depending upon the local temperature gradient) CO₂ is a gas, and readily dissolves. Below this depth, we encounter the gas hydrate phase boundary where a shell of CO₂-hydrate may be generated (7,8) on the bubble/droplet surface. Such a hydrate skin or shell, could have profound consequences; both slowing the rate of dissolution, increasing bubble lifetimes and increasing the thickness of the layer where the bulk of the CO₂ dissolves. Below about 400 m depth, pure CO₂ will exist as a liquid. Due to the relatively high compressibility of liquid CO₂ in comparison to seawater, the density ratio will invert at high pressure such that below about 2800 m depth a gravitationally stable release can be achieved (9). Release of CO₂ at depths deeper than this, may promote rapid and massive solid hydrate formation, and may lead to long oceanic residence times and effective sequestration from the atmosphere. The potential cost and technical difficulty of this deep injection scenario suggests the need to evaluate alternate injection scenarios at shallower depths.

While laboratory studies of the CO₂ clathrate-hydrate phase boundary and the solid phase have both been successful, it is difficult for a laboratory study to simulate the behavior of freely released material in motion, in a complex physical regime. Thus, several mathematical models have been devised to simulate this process and differing conclusions were reached. Holder et al. (10) modeled the behavior of a rising CO₂ plume incorporating a constantly growing film of solid hydrate. With time, this film slows the rise rate since CO₂-hydrate is more dense than either seawater or liquid CO₂, and eventually causes the combined mass to sink. Herzog et al. (3) modeled the dissolution rate of liquid CO₂ between 500 and 2000 m without the hydrate effects. They concluded that if the initial droplet radius is less than 1 cm, then complete dissolution would occur within less than 200 m. Very complete sets of model calculations incorporating plume dynamics have been carried out (3,4,11), and yet no field data exist to compare these models against.

EXPERIMENTAL

The experiments were executed beginning at 800m depth in Monterey Bay, off the coast of central California, during October 12-13, 1999, using the ROV *Ventana*. The ROV was equipped with an HDTV camera to observe the CO₂ released and the video tape recorded from this camera provides a permanent record of the work. The system captures images with a specially modified Sony HDC-750 high-definition television camera which digitizes the picture data and formats it to the SMPTE 292M HDTV interface standard with 2:1 interlace. The resolution of the images is 1035 pixels vertically and 1920 pixels horizontally which is about five times the resolution of conventional video. The image data is recorded with a Panasonic HD2000 high-definition video tape recorder without any further transcoding steps.

An earlier attempt at observing the free release of CO₂ had shown that it was impossible to maintain a CO₂ droplet cloud that was free to move in all dimensions within the field of view. Effects of the vehicle motions, strong lateral forcing due to local currents, and the similarity of appearance of a droplet of liquid CO₂ to the ubiquitous gelatinous marine organisms, all combined to frustrate continuous observation. Therefore a simple imaging box (89 cm long, 25 cm deep, and with a transparent face 30 cm wide) was constructed. It was open to the ocean at top and bottom, and mounted directly in front of the camera. The purpose of this box was to restrain lateral motions, while permitting free upward motion of the droplet plume. A meter scale within the box provided dimensional control within the imaged field. Additionally, the opaque back of the box hid the visually distracting marine snow in the background. The liquid CO₂ injector was modified slightly from that described earlier (9), and used a piston assembly, operated by the vehicle hydraulic system, to deliver 128 mL of liquid per stroke through a 1/8-inch orifice mounted on the back of the imaging box. Smaller volumes were delivered with partial strokes. A CTD instrument mounted on the ROV provided depth, temperature and salinity information for the duration of the experiment. The experiment depth was chosen to match plans for a future large-scale release of CO₂ off the coast of Hawaii (12).

With the known dimensions of the bubble box, and the meter scale attached to the rear wall, we have numerical reference points with which to quantify the images of droplets during ascent. The time at which an image was recorded was logged on the same time base as the vehicle depth (pressure), temperature, etc. Frame grabs from the HDTV video tape provide a convenient means to measure droplet dimensions by comparison to the numerical scale.

At first glance, this experiment is disarmingly simple, however experience has shown that there is more here than meets the eye. It requires the precise piloting of a 3 ton vehicle, subject to oceanic forcing in 3 dimensions, while imaging a small cloud of droplets with millimeter precision for one hour over hundreds of meters of ascent. The successful completion of this experiment is a tribute to the skill of the ROV pilots and engineers.

RESULTS

Two CO₂ release experiments were carried out. In the first experiment, the droplets rose from 800 m to 625 m depth during the course of 21 minutes, at which time the droplet escaped from the bubble box. In a second release, a droplet was followed from 800 m to 340 m depth during a period of about 1 hour. The depth versus time curve for the second release is shown in Figure 1. Small errors in positioning the bubble in the vertical center of the box are assumed to be negligible when compared to the over 400 m rise of the experiment. The temperature profile recorded during this experiment is overlain on the relevant portion of the phase diagram for CO₂ in seawater in Figure 2. Note that visual contact with the bubble was lost just below the hydrate phase boundary. The nearness of this significant boundary attracted our attention initially, but the evidence suggests that the visual loss of the bubble at this point was coincidental.

A mean ascent rate of 12.8 cm/sec was observed during the first release and 12.4 cm/sec for the second, longer, experiment. Close inspection of the data revealed a measurable increase in velocity with decreasing pressure and concomitant diminishing droplet diameter. By fitting a second-order polynomial to the depth versus time data, we were able to better estimate (from the first derivative of this equation) that the rise rate was 10.2 cm/sec initially, increasing gradually to 14.9 cm/sec just before contact was lost with the bubble. A dramatic change in rise rate coincident with the transition from droplet to bubble on crossing the liquid-to-gas phase boundary, was not observed. While the data can be smoothly fit with a second order polynomial (see Figure 1) with no evidence of a discontinuity at that point, data above this phase boundary are sparse. As the droplets rose, they shrink from dissolution, expand from pressure release, and encounter progressively warmer and less dense seawater. The net result of this complex process is the small and relatively simple to model increase in rise rate versus time that was observed.

The ideal experiment of a single purely spherical droplet proved unrealistic. Early we observed that bubble collisions were frequent, and that rafts of CO₂ droplets remained strongly attached to

each other and that these rafts persisted for very long periods. At the same time, one could recognize a distinctively shaped unit and follow it within the droplet cloud. One such unit was found which later formed a droplet pair. The changing dimensions of this droplet pair during their ascent are given in Table 1. These complex shapes, rotating in three dimensions present varying aspect ratios to the camera and frame grabs were carefully selected to remove this effect.

Occasionally, droplets collided with and stuck to the walls of the bubble box. It was possible to free the droplet with a sudden lateral ROV motion, but the possibility of mass loss to the walls, rather than by dissolution remains. Furthermore, boundary flow occurs along the walls of the bubble box as the vehicle rose, and droplets were consistently drawn to this region. In spite of these difficulties it proved possible to maintain the droplets in free flow for the greater part of the ascent suggesting that any bias due to boundary effects is small. Images, from an alternate experiment, where droplets of liquid CO₂ were allowed to rise freely while the ROV was held stationary and thus no boundary flow effects are present, are being analyzed to determine the extent of the impact of the boundary flow upon the measured rise rates.

Table 1 presents the data on droplet size versus depth. Additionally, these data are plotted versus time in Figure 3. From these observations, and literature values on the density of liquid CO₂ as a function of pressure and temperature, it is possible to calculate the mass loss with time. These results show that droplet diameter changes as a linear function of time, and gives a dissolution rate for liquid CO₂ of 3.7 $\mu\text{mol}/\text{cm}^2/\text{sec}$. This result compares well with the results of Aya et al. (5) from laboratory pressure vessel studies at 30 MPa and 4.5°C. The laboratory measurements yield a value of 1.7 or 2.8 $\mu\text{mol}/\text{cm}^2/\text{sec}$ with and without a hydrate skin, respectively. The slightly higher rate obtained in the natural environment, may be due to the lower pressures involved and the complex physical situation, or the dynamics of a rising droplet stream (13,14).

In earlier work (6,9), we have demonstrated that within the phase boundary, CO₂ hydrate forms readily, almost instantaneously, on vigorous mixing of CO₂ and seawater. In these experiments, hydrate formation is usually recognizable by a change in optical reflectivity at interface of the phases, and by a white cloudy appearance. Based upon the imagery we obtained, it is not possible to state with certainty, whether the droplets followed here maintained a hydrate skin. Immediately after injection, the droplets appear to have a stiff surface skin, and droplet rafts formed and maintained a stick like shape. As the droplets rose they became more rounded, and soon appeared to be hydrate free. It is possible that some hydrate may have formed inside the release tube and was carried out with the droplets. However it is impossible, on the basis of these observations, to say whether the dissolution rate observed was affected by a molecular boundary layer of hydrate, or whether the relatively slow dissolution is simply the result of the high degree of immiscibility between liquid CO₂ and seawater.

The choice of a scenario for the long term sequestration of anthropogenic CO₂, either via a rising stream of CO₂, or via the formation of a sinking plume with hydrate formation (9) has yet to be made. The results presented here should allow a more accurate prediction of the CO₂/pH field, and the environmental effects, surrounding an injection point. However, a critical property for the longer term will be the effectiveness of the process in terms of sequestration. For example, the depths chosen here cover the 27.3 - 26.8 (σ_θ) isopycnal surfaces. While the 26.8 surface is the most dense seawater to outcrop seasonally at the surface in the North Pacific, Warner et al. (15) have recently mapped the ventilation age of this surface demonstrating that it was relatively recently (12-32 years) exposed to contact with the atmosphere. This probably represents the shallowest depth at which disposal in this ocean basin is likely to be effective as a sequestration option, although other shallow disposal scenarios have also been considered (13,14).

The small-scale ROV experiments described here are a "first effort" to evaluate these processes, and appear to offer an effective way to approach the problem without the costs and problems associated with larger-scale releases. We were not yet able with these small quantities to easily simulate some of the changes in local seawater density, and "peeling" of the plume predicted by large scale fluid dynamic modeling (11). At the same time, it should be recognized that the results reported here pertain to isolated bubbles moving in a more or less undisturbed ocean. Differences with the large-scale releases will no doubt be found. It is not only possible to extend these studies to include biological effects (16) but it is also desirable and this work is in progress.

ACKNOWLEDGEMENTS

The authors would like to thank the Captain and crew of the RV *Point Lobos*, and the pilots of the ROV *Ventana*. Without their skilled support, this research would not have been possible. This work was supported by a grant to MBARI from the David and Lucile Packard Foundation.

REFERENCES

1. C. Marchetti, *Climate Change* **1**, 59 (1977).
2. N. Handa and T. Ohsumi, *Direct Ocean Disposal of Carbon Dioxide* (Terra Scientific Publishing, Tokyo, 1995).
3. H. Herzog, D. Golomb, S. Zemba, *Envir. Prog.* **10**, 64 (1991).
4. H. Drange, P. Haugan, *Tech. Rep. 54, NERSC* (1992).
5. I. Aya, K. Yamane, H. Nariai, *Energy* **22**, 263 (1997).
6. P. G. Brewer, F. M. Orr, Jr., G. Friederich, K. A. Kvenvolden, D. L. Orange, *Energy Fuels* **12**, 183 (1998).
7. E. D. Sloan Jr., *Clathrate Hydrates of Natural Gases* (Dekker, New York, 1990).
8. W. J. North, V. R. Blackwell, J. J. Morgan, *Environ. Sci. Technol.* **32**, 676 (1998).
9. P. G. Brewer, G. Friederich, E. T. Peltzer, and F. M. Orr, Jr., *Science* **284**, 943 (1999).
10. G. D. Holder, A. V. Cugini, R. P. Warzinski, *Environ. Sci. Technol.* **28**, 276 (1995).
11. G. Alendal, H. Drange, *J. Geophys. Res.* In Press.
12. E. Adams, H. Herzog, *Tech. Rept., MIT* (1998).
13. P. Haugan, H. Drange, *Nature* **357**, 318 (1992).
14. R. Clift, J. R. Grace, M. E. Weber, *Bubbles, Drops and Particles* (Academic Press, New York, 1978).
15. M. J. Warner, J. L. Bullister, D. P. Wisegarver, R. H. Gammon, R. F. Weiss, *J. Geophys. Res.* **101**, 20,525 (1996).
16. M. N. Tamburri, E. T. Peltzer, G. E. Friederich, I. Aya, K. Yamane, P. G. Brewer, *Mar. Chem.*, In Press.

Table 1

Measured Liquid CO₂ Droplet Characteristics during Ascent from 800m Depth

Elapsed Time (min)	Depth (m)	Temp. (°C)	Droplet Diameter (cm)		CO ₂ Density (g/cc)	Amount of CO ₂ (millimoles)		Rise Rate (cm/s)
			(a)	(b)		(a)	(b)	
0	804.5	4.398	1.10		0.9423	14.92		10.2
14.23	706.3	4.740	0.75		0.9310	4.67		11.3
23.13	649.1	4.994	0.60	1.10	0.9235	2.37	14.63	12.0
29.82	602.1	5.165	0.45	0.90	0.9171	0.99	7.96	12.5
43.08	496.8	5.449	0.20	0.80	0.9021	0.09	5.50	13.5
49.73	447.3	5.995		0.45	0.8910		0.97	14.0
61.65	341.2	7.291		0.25	0.8632		0.16	14.9

The initial droplet tracked (a) was joined at about 650 m depth by a second, larger, bubble (b) which became attached. No change in rise rate could be detected due to the attachment, and the changing size of each droplet could be independently determined. The mean density of liquid CO₂ during the rise of the droplets was 0.92 (a) and 0.90 (b), respectively. Thus, a 1 cm³ droplet contains 21.1 (a) or 20.4 (b) millimoles CO₂. We calculate the dissolution rate (Γ) from the slope of:

$$(r_t - r_0) = -V_m \times \Gamma \times (t - t_0), \quad [1]$$

where V_m is the specific volume (mmol/cm³), r_0 and r_t are initial droplet radius and droplet radius at time t , and t_0 and t are initial time and the time elapsed since t_0 . The observed dissolution rate was 3.7 $\mu\text{mol}/\text{cm}^2/\text{sec}$.

The rise rate was determined by fitting a second-order polynomial to depth versus time to obtain:

$$Z_t = -2.250 \times 10^{-2} \times t^2 - 6.145 \times t + 799.2, \quad [2]$$

then taking the first derivative of equation [2] to yield the rise rate at time, t :

$$R_t = -0.0450 \times t - 6.145. \quad [3]$$

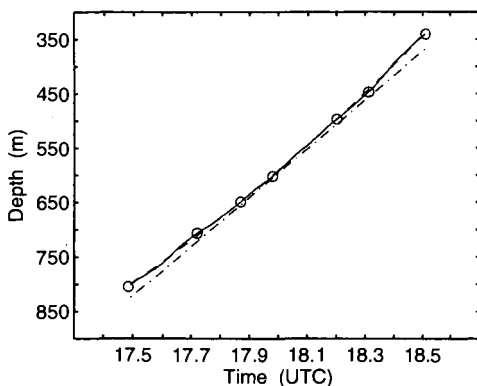


Figure 1. Plot of the observed ROV depth vs time for the second CO₂ release (solid line) and selected droplets (o). The mean rise rate for this release is shown as the dot-dash line tangent to the mid-point of the data curve. The dashed line is the second order polynomial fit to depth.

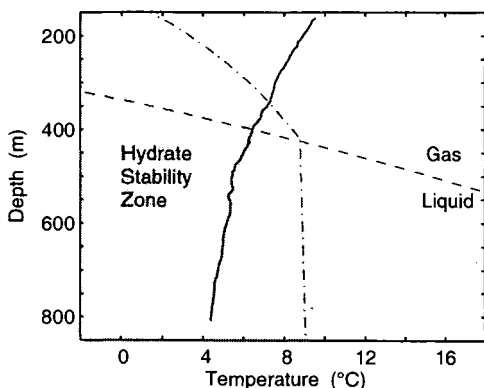


Figure 2. The observed ocean temperature profile recorded during the droplet rise experiments, overlaid on the CO₂ phase diagram for seawater. While the injection point is far inside the region for hydrate formation, the droplet crossed the liquid-to-gas phase boundary at about 400 m depth, and visual contact with the droplet was lost at about 340 m depth.

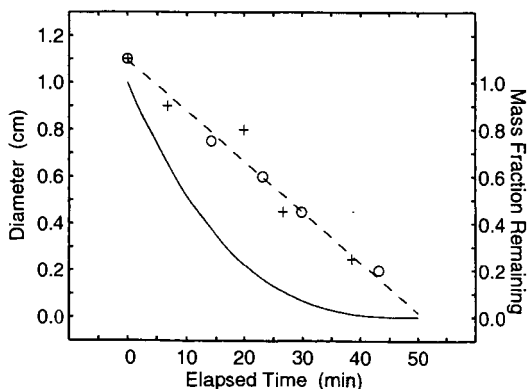


Figure 3. Plot of the changing droplet diameter with time, and remaining mass fraction of the droplets. The droplet size derived from HDTV video analysis, as listed in Table 1, is shown by circles (a) and crosses (b), respectively. The dashed line indicates the trend of diameter versus time calculated from equation (1) with a dissolution rate of $3.7 \mu\text{mol}/\text{cm}^2/\text{sec}$. The solid line shows the calculated remaining mass fraction relative to the initial mass of the CO₂ droplets.

ANALYTICAL AND EXPERIMENTAL STUDIES OF DROPLET PLUMES WITH APPLICATION TO CO₂ OCEAN SEQUESTRATION

E. Eric Adams, Brian C. Crouse, Timothy H. Harrison, and Scott A. Socolofsky
Dept. Civil & Environ. Engrg., Massachusetts Institute of Technology,
Cambridge, MA 02139

1. Abstract

This paper describes a numerical model of a steady-state plume in linear stratification driven by a buoyant dispersed phase, such as bubbles or droplets. The model was developed specifically to simulate CO₂ sequestration plumes. It extends the hybrid double-plume model of Asaeda & Imberger (1993) by incorporating droplet dynamics (dissolution, hydrate formation, and phase changes), by introducing a self-regulating detrainment criterion, and by allowing multiple intrusions to overlap. The model is calibrated to data from the literature and is applied to study the sensitivity of a CO₂ plume to ambient stratification.

2. Introduction

Several techniques for transferring CO₂ to the deep ocean have been proposed; buoyant droplet plumes injected around 1000 m depth are the simplest and least costly (Adams & Herzog 1996). Although the oceans and atmosphere will eventually equilibrate (on the order of 1000 years), the intent of such a sequestration strategy is to minimize atmospheric CO₂ concentrations over the next few hundred years, by which point CO₂ emissions will have significantly decreased (Adams & Herzog 1996). This paper examines the design of such a CO₂ injection.

This paper presents a numerical model for a two-phase plume in stratification that extends the hybrid double-plume model of Asaeda & Imberger (1993). The model currently neglects the effects of a crossflow in order to minimize the number of dynamic processes involved. This is deemed acceptable since the no-current case probably represents a worst-case scenario in terms of dilution of the dissolved CO₂. Because the dissolution of CO₂ increases the density of the seawater, there is a feedback on the plume dynamics. After presenting the model, this paper explores the relative importance of stratification and CO₂ dissolution for controlling the resultant plume structure.

3. Model Formulation

The spatial evolution of a two-phase plume in stratification is controlled by four primary processes: buoyant forces acting upon the droplets and plume water, dissolution of the droplets, turbulent entrainment of ambient water into the plume, and buoyant detrainment, called peeling. Qualitative two-phase plume behavior depends on the values of the droplet buoyancy flux, B , droplet slip velocity, u_s , and the strength of the ambient density stratification, N . Asaeda & Imberger (1993) and Socolofsky (in prep.) have identified four classes of two-phase plumes in stratification, illustrated in Figure 1. Type 1 plumes act like plumes in unstratified surroundings, flowing to the water surface without interruption. Type 2 plumes exhibit one or more intermediate peeling events, where plume water is stripped from the rising droplets by buoyant forces. The peeled water descends until it becomes forms a neutrally buoyant intrusion flow. Type 1* is a variant of Type 2 where the droplet slip velocity is low enough that the droplets partially peel along with the plume water. A Type 3 plume occurs when the droplet slip velocity is very high, so that the droplet core does not effectively transport ambient fluid. The progression from Type 1* to Type 3 can be correlated with the dimensionless slip velocity (Socolofsky, in prep.),

$$U_N = \frac{u_s}{(BN)^{1/4}} \quad (1)$$

The vertical evolution of plume structure can be predicted with an integral model. Integral models describe the plume flow as a one-dimensional problem by assuming a profile shape independent of height for each variable describing a plume property. Although this similarity assumption is not strictly valid for a two-phase plume in stratification, models based on similarity have been successful (Asaeda & Imberger 1993, Wüest et al. 1992, Turner 1986, McDougall 1978). Here, we choose top-height profiles (variables are assumed constant over the plume width) for both the inner, rising plume of water and droplets, and for the outer, falling annular plume of water only. Asaeda & Imberger (1993) introduced this type of double plume.

We formulate the model in terms of the governing flux variables. The mass flux of bubbles, W_b , is given by their number flux, N_b , their nominal diameter, d_b , and their density, ρ_b , yielding

$$W_b(z) = \frac{1}{6} \pi d_b^3(z) N_b \rho_b(z) = Q_b(z) \rho_b(z) \quad (2)$$

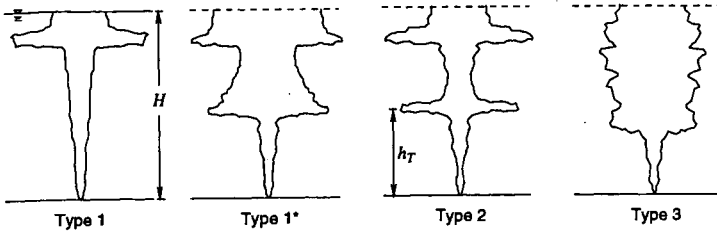


Figure 1. Schematic of characteristic two-phase plume behavior in stratification.

The size and density of bubbles are tracked in a bubble sub-model that accounts for dissolution, hydrate formation and phase changes. Denoting X as the cross-sectional fraction of the inner plume occupied by bubbles, we define the volume flux, Q , of plume water as

$$Q_i(z) = \int_0^b (1 - X(z)) u_i(z) 2\pi r dr = \pi b_i^2 u_i \quad (3)$$

where u is the average water velocity and b is the plume width. The subscript i indicates an inner-plume value. The momentum flux, M , includes the momentum of both the bubbles and the droplets

$$M_i(z) = \gamma \int_0^b (1 - X(z)) u_i^2(z) \rho_i(z) 2\pi r dr + \gamma \int_0^b X(z) (u_i(z) + u_b(z))^2 \rho_b 2\pi r dr \quad (4)$$

where u_b is the bubble slip velocity and γ is a momentum amplification term, first introduced by Milgram (1983), that accounts for the fact that the model formulation implicitly ignores turbulent momentum transport. Because $X \ll 1$ and $u_b = O(u_i)$, the second term in (4) can be ignored giving $M_i = \gamma \rho_i \pi b_i^2 u_i^2 = \gamma \rho_i Q_i u_i$.

The buoyant forces generating the plume result from changes in density. For this model, density is tracked through changes in salinity flux, S , heat flux, J , and the dissolved CO_2 flux, C . The salinity flux is defined from the local plume salinity, s , such that

$$S_i(z) = Q_i(z) s_i(z) \quad (5)$$

The heat flux of the plume is defined from the local water temperature, T , yielding

$$J_i(z) = Q_i(z) \rho_i c_p(z) T_i(z) \quad (6)$$

where c_p is the heat capacity of the fluid. Finally, the dissolved CO_2 flux is defined from the local dissolved CO_2 concentration, c ,

$$C_i(z) = Q_i(z) c_i(z) \quad (7)$$

Thus, (2) through (7) define the model state variables for the inner plume.

The state variables for the outer plume are nearly identical. The primary difference is that, because the outer plume is assumed to be annular, the volume flux of the outer plumes is defined as

$$Q_o(z) = \pi (b_o^2 - b_i^2) u_o \quad (8)$$

where the subscript, o , indicates an outer plume value. Defining z as the upward spatial coordinate and specifying that the outer plume flow downward, the velocity u_o is negative and u_i is positive. Using (8) and changing the subscripts in (2) to (7) from i to o yield the flux equations for the outer plume.

The plume develops by exchanging fluid with the ambient and by exchanging fluid between the inner and outer plumes. The entrainment hypothesis, introduced by Morton et al. (1956), states that the entrainment flux across a turbulent shear boundary is proportional to a characteristic velocity in the turbulent layer. In this model, we have defined three entrainment fluxes: E_i entrains from the ambient or from the outer plume into the inner plume, E_o entrains from the inner plume into the outer plume, and E_a entrains from the ambient into the outer plume. The entrainment relationship for counterflows is not well known. Here, we adopt the relationship used by Asaeda & Imberger (1993):

$$E_i(z) = 2\pi b_i \alpha_i (u_i - u_o) \quad (9)$$

$$E_o(z) = 2\pi b_o \alpha_o u_o \quad (10)$$

$$E_a(z) = 2\pi b_o \alpha_a u_o \quad (11)$$

where the α 's are entrainment coefficients.

The final exchange equation accounts for buoyant detrainment, which has been modeled in a variety of ways. Liro (1992) assumed that a fixed fraction of plume fluid was ejected when the net buoyancy flux across the plume approached zero. Asaeda & Imberger (1993) assumed that all of the plume fluid detrained when the net momentum approached zero. Based on experiments, peeling is better predicted when the net momentum approaches zero. For this model, a self-regulating peeling criterion is introduced. We know that peeling occurs when the drag from the bubbles can no longer support the negative buoyancy of the fluid. The simplest parameterization that behaves similarly to experiments gives the peeling flux as

$$E_p(z) = \varepsilon \left(\frac{u_b(z)}{u_i(z)} \right)^2 \left(\frac{B_i(z)}{u_i^2(z)} \right) \quad (12)$$

where ε is a non-dimensional fitting parameter of order 0.01, and B is the buoyancy flux, defined as

$$B_i(z) = gQ_i(z) \frac{\rho_a(z) - \rho_l(z)}{\rho_l} \quad (13)$$

where ρ_a is the ambient density. The relationship in (12) makes it easier for outer plumes to overlap and makes it possible to simulate the continuous peeling nature of Type 3 plumes, which were first defined by Asaeda and Imberger (1993).

With these definitions, the plume conservation equations can be readily defined. From mass conservation, we have:

$$\frac{dQ_i}{dz} = E_i + E_o + E_p \quad (14)$$

$$\frac{dQ_o}{dz} = E_i + E_o + E_p + E_a \quad (15)$$

Momentum conservation states that the momentum changes in response to the applied forces, which gives the following equations

$$\frac{dM_i}{dz} = g \left(\frac{Q_o}{(u_i + u_b)} (\rho_a - \rho_b) + \pi b_i^2 (\rho_a - \rho_l) \right) + E_i \rho_o u_o + E_o \rho_l u_i + E_p \rho_l u_i \quad (16)$$

$$\frac{dM_o}{dz} = -g\pi(b_o^2 - b_i^2)(\rho_a - \rho_o) + E_i \rho_o u_o + E_o \rho_l u_i + E_p \rho_l u_i + E_a \rho_a u_a \quad (17)$$

The conservation of salt, heat and dissolved CO₂ flux follow from the mass conservation equation, yielding for the inner plume:

$$\frac{dS_i}{dz} = E_i s_o + E_o s_i + E_p s_i \quad (18)$$

$$\frac{dJ_i}{dz} = c_p \rho_l (E_i T_o + E_o T_i + E_p T_i) + \frac{dW_b}{dz} \Delta H_{diss} \quad (19)$$

$$\frac{dC_i}{dz} = E_i c_o + E_o c_i + E_p c_i \quad (20)$$

and for the outer plume:

$$\frac{dS_o}{dz} = E_i s_o + E_o s_i + E_p s_i + E_a s_a \quad (21)$$

$$\frac{dJ_o}{dz} = c_p \rho_l (E_i T_o + E_o T_i + E_p T_i + E_a T_a) \quad (22)$$

$$\frac{dC_o}{dz} = E_i c_o + E_o c_i + E_p c_i + E_a c_a \quad (23)$$

The last term in (19) accounts for the energy released by dissolving CO₂. The densities ρ_l and ρ_o are determined by an equation of state which is a function of s , T , and c . dW_b/dz is calculated by the bubble sub-model.

The model begins with integration of the inner plume from the point of release to the point where the droplets disappear or the water surface is reached. Once the inner plume integration is complete, the outer plume segments are integrated. The integration of each outer plume section continues until the momentum flux approaches zero. Then, the next outer plume section is initialized and integrated. This cycle repeats until the solution converges to a steady result (typically 10 iterations).

4. Results

Literature data were available for an unstratified bubble plume and for a single-phase plume ($u_b=0$) in stratification. For both these cases the outer plume did not develop, so only values for α_i could be calibrated. Data for the unstratified case were from Milgram (1983) for a 50 m deep spring. The model matched the trend and magnitude of the measured plume velocities for a value of $\alpha_i =$

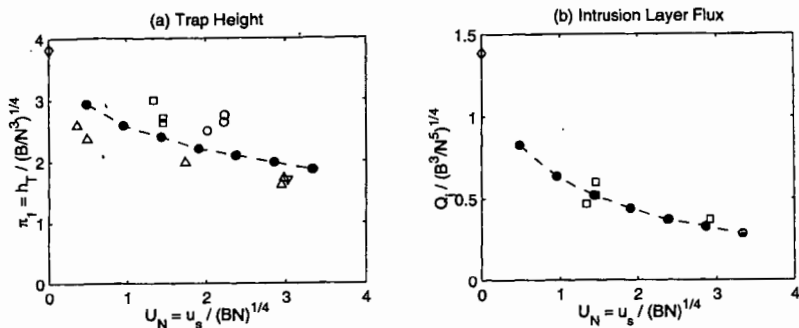


Figure 2. Model predicted (a) trap height and (b) intrusion layer volume flux versus experimental data. Up and down triangles are from Reingold (1994), open circles are from Asaeda and Imberger (1993), right-pointing triangles are from Lemckert and Imberger (1993), and squares are from experiments described in Socolofsky (in prep.). Model predictions are represented by the filled circles.

0.12. In the stratified case, the trap height relationship $h_T = 3.8(B/N^3)^{1/4}$ was tested. The model reproduced the scale-dependence of h_T on B and N for $\alpha_i = 0.11$.

Additional calibration data for two-phase plumes in stratification were available from Socolofsky (in prep.). The height of the first peeling event, h_T , and the volume flux in the resulting intrusion, Q_i , can be correlated with U_N . Calibrating to the trap-height relationship gives values of $\alpha_i = 0.07$, $\alpha_o = 0.11$, and $\alpha_s = 0.11$. Figure 2 shows the model predictions for trap height and intrusion layer flux, compared to experimental data.

The ambient density gradient, characterized by the buoyancy frequency, varies somewhat with geographic location and strongly with depth. To investigate the model sensitivity to stratification, a base-case CO_2 injection scenario was defined. Table 1 summarizes the base case along with scenarios featuring decreased and increased stratification.

Variable	Decreased Stratification	Base Case	Increased Stratification
Release Depth	800 m	800 m	800 m
Droplet Diameter	0.5 cm	0.5 cm	0.5 cm
Droplet Density	940 Kg/m^3	940 Kg/m^3	940 Kg/m^3
Flow rate	1.1 L/s	1.1 L/s	1.1 L/s
Buoyancy Frequency	0.0016 s^{-1}	0.0032 s^{-1}	0.0064 s^{-1}

Table 1. Simulation scenarios for CO_2 sequestration sensitivity analysis.

Figure 3 shows the model results for the three sequestration scenarios in Table 1. Although the total plume rise heights are about the same (the bubbles completely dissolve at the same height), the intrusion levels and fluxes differ. The volume flux to the intrusion layers decreases with increasing stratification because their descent is arrested more quickly in higher stratification, which leads to less cumulative entrainment and less total dilution. The mean concentration of excess CO_2 and the resulting change in pH in the intrusions are summarized in Table 2.

Case	Intrusion excess CO_2
Decreased stratification	0.03 Kg/m^3
Base case	0.06 Kg/m^3
Increased stratification	0.13 Kg/m^3

Table 2. Intrusion excess CO_2 concentration and change in pH for the three cases simulated.

The near-field dilution of the CO_2 reported in Table 2 is controlled by the competition between the stratification and the solution density effect of the CO_2 . Over the range of buoyancy frequencies sampled, the concentration of CO_2 in the intrusion layers is nearly proportional to the buoyancy frequency.

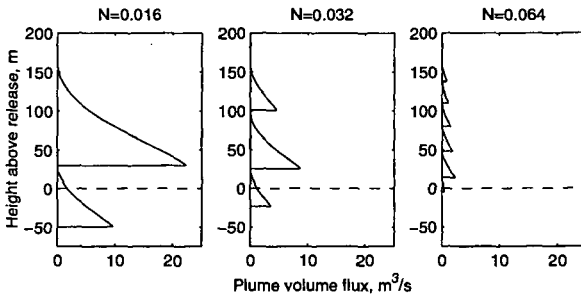


Figure 3. Sensitivity of plume structure to ambient stratification. The solid lines represent the volume flux profiles of the outer plume sections. The inner plume volume flux profiles are omitted for clarity.

5. Conclusions

A numerical model has been presented that extends our modeling abilities for a buoyant CO₂ plume in the deep ocean. The newly introduced detrainment relationship (12) provides a convenient numerical solution for downdraught flows that overlap, as is the case for CO₂ plumes. Although the entrainment relationship for the resulting counterflow is not well understood, the density feedback of the CO₂ dissolution provides a large enough driving force that the outer plume dominates the structure, and the dilution in the outer plume becomes insensitive to reasonable values for the entrainment coefficients. Thus, the near-field dilution of a CO₂ plume is controlled by the balance between the negative buoyancy of the dissolving CO₂ and the stratification, rather than by the buoyancy of the bubbles.

6. Acknowledgements

This work was supported by the MIT Sea Grant College Program, the National Energy Technology Laboratory of the U.S. Department of Energy, and the Deep Spills Task Force, comprised of the Minerals Management Service of the U.S. Department of Interior and a consortium of 13 member oil companies of the Offshore Operations Committee.

7. References

- Adams, E. E. & Herzog, H. J. (1996), Environmental impacts of ocean disposal of CO₂, Technical Report MIT-EL 96-003, Energy Laboratory, MIT.
- Asaeda, T. & Imberger, J. (1993), 'Structure of bubble plumes in linearly stratified environments', *J. Fluid Mech.* **249**, 35-57.
- Lemckert, C. J. and Imberger, J. (1993), 'Energetic bubble plumes in arbitrary stratification', *J. Hydr. Engrg.* **119**, 680-703.
- Liro, C. R., Adams, E. E., Herzog, H. J. Modeling the Release of CO₂ in the Deep Ocean, Technical Report MIT-EL 91-002, Energy Laboratory, MIT.
- McDougall, T. J. (1978), 'Bubble plumes in stratified environments', *J. Fluid Mech.* **85**, 655-672.
- Milgram, J. H. (1983), 'Mean flow in round bubble plumes', *J. Fluid Mech.* **133**, 345-376.
- Morel, F. M. M. & Hering, J. G. (1993), *Principles and Applications of Aquatic Chemistry*, Wiley-Interscience, New York.
- Morton, B., Taylor, G. I., & Turner, J. S. (1956), 'Turbulent gravitational convection from maintained and instantaneous sources', *Proc. R. Soc. London Ser. A* **234**, 1-23.
- Reingold, L. S. (1994), An experimental comparison of bubble and sediment plumes in stratified environments, M.S. Thesis, Dept. of Civ. & Environ. Engrg., MIT, Cambridge, MA
- Socolofsky, S. A., Crouse, B. C. & Adams, E. E. (2000), 'Bubble and droplet plumes in stratification 1: Laboratory studies' in Proc. IAHR 5th Int. Symp. Strat. Flow, Vancouver, BC, July 10-13.
- Socolofsky, S. A. (in prep.), Laboratory Experiment of Multi-phase Plumes in Stratification and Crossflow, Ph.D. Thesis, Dept. Civ. & Environ. Engrg., MIT, Cambridge, MA.
- Turner, J. S. (1986), 'Turbulent entrainment: the development of the entrainment assumption, and its application to geophysical flows', *J. Fluid Mech.* **173**, 431-471.
- Wüest, A., Brooks, N. H. & Imboden, D. M. (1992), 'Bubble plume model for lake restoration', *Wat. Resour. Res.* **28**, 3235-3250.

EXPERIMENTS TO INVESTIGATE CO₂ OCEAN SEQUESTRATION

Stephen M. Masutani¹, Masahiro Nishio², Guttorm Alendal³, and Gérard C. Nihous⁴

¹University of Hawaii, Hawaii Natural Energy Institute
2540 Dole Street, Holmes 246, Honolulu, Hawaii 96822 USA

²Mechanical Engineering Laboratory, Department of Energy Engineering
1-2 Namiki, Tsukuba, Ibaraki 305-8564 JAPAN

³Nansen Environmental & Remote Sensing Center
Edvard Griegsvei 3A, 5037 Solheimsvike, Bergen N-5037 NORWAY

⁴Pacific International Center for High Technology Research
2800 Woodlawn Drive, Suite 180, Honolulu, Hawaii 96822 USA

KEYWORDS: CO₂; ocean sequestration; environmental impact

ABSTRACT

An international collaboration to investigate the sequestration of CO₂ in the deep ocean was initiated in December 1997. The program is being funded by agencies of the governments of Japan, the U.S., Norway, Canada, and Australia; and Asea Brown Boveri (ABB) of Switzerland. The investigation comprises both experimental and modeling components. During the first phase of the program which runs through March 2002, a field experiment will be conducted in the summer of 2001 in which liquid CO₂ will be injected through various nozzles at a depth of approximately 800 m in the ocean at flow rates ranging from about 0.1 to 1 kg/s. Data will be obtained to develop and validate models that can be applied to predict induced changes to sea water chemistry. This paper describes the planned field experiment and presents selected results from laboratory and modeling studies that have been conducted to support the field experiment.

INTRODUCTION

Anthropogenic emissions of greenhouse gases may precipitate significant changes in global climate. The magnitude and extent of these changes are being actively investigated and debated. Carbon dioxide (CO₂) currently is the most important of these gases due to the preponderant quantities being released into the atmosphere by the combustion of fossil fuels. The latest Intergovernmental Panel on Climate Change (IPCC) assessment indicates that more than 80% of the heat trapping potential of anthropogenic greenhouse gas emissions is associated with CO₂ (UNFCCC, 1997).

International negotiations to establish practices that will stabilize atmospheric concentrations of greenhouse gases have been underway since 1992. In 1997, the Kyoto Protocol established legally-binding greenhouse gas emissions targets for Annex I industrialized countries. For the majority of these countries, the Protocol mandates that a 5% to 8% reduction of CO₂ emissions from 1990 levels be achieved sometime between 2008 and 2012 (UNFCCC, 1998).

Although renewables are being promoted to reduce greenhouse gas emissions, a major transition away from fossil fuels appears unlikely in the near-term. At present, practical and economic factors favor approaches such as increasing the percentage of electricity generated by nuclear power plants, energy conservation, switching from coal and oil to a lower-carbon fuel such as natural gas, and upgrading the efficiencies of fossil fuel energy systems.

Another approach to reduce greenhouse gas emissions into the atmosphere from fossil fuel combustors is to develop techniques to recover, reuse, and/or dispose of the 'fossil' CO₂ released by these devices. One technique that has emerged as a primary candidate for the control of atmospheric carbon emissions involves extraction of CO₂ from flue gases, followed by liquefaction and sequestration underground or in the deep ocean.

Removal and liquefaction of CO₂ from the effluent streams of industrial fossil fuel combustors can be accomplished utilizing existing technologies, albeit at substantial cost (Mori *et al.*, 1993; Herzog *et al.*, 1996). The technical viability of the concept as a means to stabilize emissions therefore depends on whether long term (i.e., of the order of centuries) sequestration of the captured CO₂ from the atmosphere can be achieved. Given the limited range of reuse options, huge quantities of CO₂ will need to be disposed of in an environmentally safe, and cost effective manner. Disposal in the ocean and in subterranean sites such as deep coal seams, spent gas and

oil wells, aquifers, salt domes, and rock caverns has been considered. While geological storage has the potential for very long term sequestration from the atmosphere—of the order of millennia—the world's oceans have a larger capacity to absorb CO₂. It has been estimated that the oceans can accept orders of magnitude more CO₂ than the amount that would be released by oxidation of all known recoverable fossil fuels reserves

The oceans currently remove at least 2 Gigatonnes (i.e., 2×10^{12} kg) of the 6-7 Gigatonnes of carbon released annually by human activity into the atmosphere. Over time, about 80% of this anthropogenic carbon is expected to find its way into the oceans. The slow process of exchange between the surface and deep zones of the ocean, however, constitutes a bottleneck that results in the accumulation of CO₂ in the atmosphere. While direct injection of CO₂ into the depths of the ocean would circumvent this bottleneck, associated impacts on the marine environment in the region surrounding the discharge need to be investigated. CO₂ readily goes into solution in sea water to form dissolved CO₂, and carbonate and bicarbonate ions (Millero & Sohn, 1992). One consequence of this process, however, is a depression of pH. While calcareous materials present in the deep ocean will buffer this effect, and dilution should limit acute changes in sea water chemistry, accurate quantification of these changes is not possible with existing data and models.

Laboratory experiments to investigate CO₂ ocean disposal phenomena have been pursued for over a decade (Masutani & Nihous, 1997). While these experiments have yielded important information, they will never be able to simulate completely the complex, large-scale discharge process. To address this limitation, an R&D program comprising a sequence of three field experiments of increasingly larger scale was authorized via a cooperative agreement signed in December 1997 by representatives of the Governments of Japan, the United States, and Norway. Since its inception, the Governments of Canada and Australia, and Asea Brown Boveri (ABB) of Switzerland, a private sector entity, have joined the program as sponsors.

EXPERIMENTAL PROGRAM

The experimental program has been described previously by Masutani & Nihous (1999), and Masutani (2000). Under the cooperative agreement, three separate field experiments will be conducted in the following sequence: (1) short-term tests of direct release of pure CO₂ at a depth of about 800 m at an open ocean site; (2) longer duration experiments to evaluate acute and chronic biological impacts; and (3) operation of an ocean sequestration test facility over several years to obtain extended-term operational data. Work on the first phase (short-term) field experiment officially was initiated following the signing of the cooperative agreement in December 1997 and will continue through the spring of 2002.

Liquid CO₂ released in the deep ocean is hydrodynamically unstable and will break up into a dispersed droplet phase. Within the depth regime that is accessible using existing pipeline technologies (say, $\leq 1,500$ m), the CO₂ droplets are buoyant and will rise as a plume through the density-stratified water column. A thin, solid hydrate phase may form on the droplet surface that impedes, but does not prevent dissolution (Aya & Yamane, 1992; Teng *et al.*, 1995; Hirai *et al.*, 1995). Sea water will be entrained into the rising droplet plume and transported upward to depths where the ambient water is less dense. Dissolution of CO₂ increases the density of the sea water in the plume. At various points in its ascent, heavy, CO₂-enriched sea water peels away from the plume and subsides to a level of neutral buoyancy (Liro *et al.*, 1992). This CO₂-enriched sea water subsequently is diluted and dispersed by ocean turbulence and currents.

The complex dynamics of the droplet plume in the stratified deep ocean, the effects of hydrates, and dilution and dispersion of CO₂-enriched sea water must be understood in order to address the issues of marine environmental impacts and the effectiveness of sequestration. Models currently are not capable of simulating the behavior of the CO₂ effluent with an acceptable level of confidence, and the fundamental physics of the process are not completely understood.

During the first field experiment, data will be obtained on changes induced in sea water chemistry by the release of pure CO₂. A preliminary sampling of biota and a study of the effects of the discharged CO₂ on naturally occurring bacteria populations also are planned. The specific objectives are:

1. investigate CO₂ droplet plume dynamics through qualitative flow visualization (using mobile video cameras) and quantitative measurements of velocity and pH in the plume and on its margins;
2. clarify the effects of hydrates on droplet dissolution through visualization of the droplet phase and measurements of the vertical extent of droplet rise using scalar indicators (either pH or other added tracers);

3. trace the evolution of CO₂-enriched sea water that peels from the plume by mapping the velocity and relevant scalar (e.g., pH or dissolved inorganic carbon) fields; and
4. assess potential impacts on marine biota by quantifying variations in bacterial biomass, production, and growth efficiency associated with induced changes in seawater pH.

Experiments are scheduled for the summer of the year 2001 at a facility on the west coast of the island of Hawaii. A series of tests with combined duration of about 40 hours will be conducted over two weeks. During these tests, pure liquid CO₂ will be pumped from refrigerated storage tanks installed on a ship to a depth of about 800 m through a small suspended conduit (3 to 6 mm i.d.). The liquid CO₂ will be discharged through different injectors installed at the end of the conduit. The discharge rate will be varied between 0.1 kg/s and 1 kg/s. A range of CO₂ discharge conditions (i.e., mass flow rate; injection velocity; droplet size) will be examined.

Data will be collected employing both fixed and mobile diagnostics. A video system mounted on an ROV (remotely-operated vehicle) will provide flow images of the CO₂ droplet plume. pH sensors and acoustic current profilers will be moored on the sea floor along with the ROV transponders to monitor ambient conditions. Detailed mapping of the scalar and velocity fields will be performed utilizing ROV-mounted instruments that will include conventional salinity, temperature, and pH probes. The ROV will collect data along a three dimensional survey path through the droplet plume and the region of CO₂-enriched sea water generated by the discharge. Water and sediment samples will be collected for chemical and biological analysis and CTD casts will be performed to supplement the data obtained with the moored arrays and ROV.

RESULTS

To support the planning and design of the 2001 field experiment, oceanographic surveys and modeling and laboratory studies are being conducted. A brief overview of this work is provided in this section.

An oceanographic survey of the experimental site off the west coast of the island of Hawaii was conducted during the first week of August 1999. A second survey is scheduled for October 2000. Data has been obtained that: (1) documents the background currents and sea water chemistry and density, and quantifies spatial and temporal variations of these quantities; (2) characterizes ambient bacterial production rates and their response to pH variations; and (3) characterizes the local benthic communities. During the survey, the performance of three methods to measure pH—a conventional glass electrode on the CTD; a novel IS-FET (ion specific field effect transistor) instrument; and shipboard photometric analysis of sea water samples—were compared and evaluated. Accurate and reliable measurements will be critical during the 2001 field experiment, since pH is a primary indicator of the released CO₂. Selected results from the 1999 oceanographic survey have been posted on the project website (<http://www.co2experiment.org>).

Laboratory experiments are being conducted to evaluate injectors and to address concerns related to flow instabilities, flow rate control, and hydrate blockage. Tests are being performed in pressure facilities at the Southwest Research Institute and the University of Hawaii (UH). Figures 1 and 2 present representative video frames obtained in a series of experiments at UH in which liquid CO₂ was pumped into a large pressure vessel to assess the performance of a multiple orifice prototype injector and to investigate hydrate blockage phenomena.

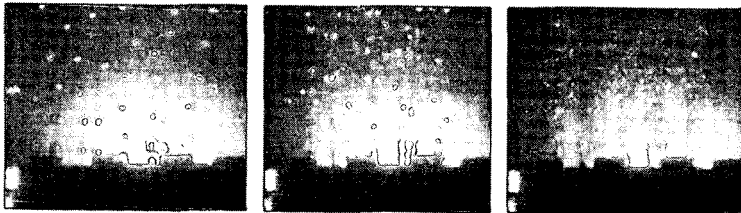


Figure 1 CO₂ injection into a laboratory pressure vessel. The frames show injection at different flow rates through an injector consisting of seven 2 mm diameter ASME sharp-edged orifices; water pressure = 56 bar; water temperature = 2°C.

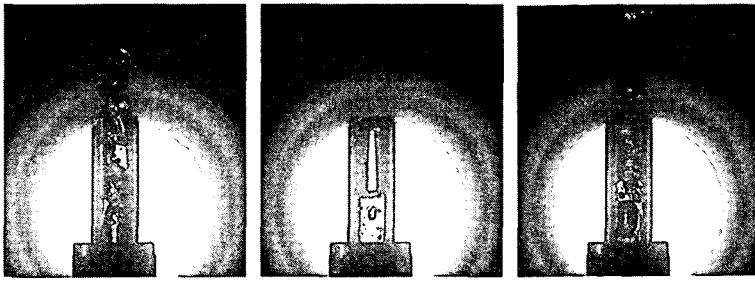


Figure 2 Liquid CO₂ and water flow through a clear nozzle used to investigate hydrate blockage; water pressure = 56 bar; water temperature = 3°C.

Estimates of the height of the droplet plumes and changes in the pH and dissolved CO₂ fields induced by the injection of liquid CO₂ during the experiment are needed to optimize the test plan and instrumentation; and for the Environmental Assessment report and permit applications. Several modeling activities have been pursued by the project team. The most sophisticated supercomputer model produces time-dependent spatial distributions of pH and dissolved and undissolved CO₂ concentrations for user-specified injection scenarios (Alendal *et al.*, 1998). Figure 3 presents one set of results for the Hawaii experiment site when liquid CO₂ is injected at 790 m at a rate of 1 kg/s in a 5 cm/s cross current. It is assumed that the injector produces a monodispersion of 14 mm diameter droplets. The mass transfer coefficient used in these simulations approximates the dissolution of liquid CO₂ droplets covered with a hydrate film. The results imply that the droplet plume will rise less than 150 m before dissolving completely. The lowest pH detected by the simulation for this case was about 6.1 (ambient pH = 7.5).

SUMMARY

A research program to investigate the feasibility of sequestering CO₂ in the deep ocean as a means to reduce the build-up of greenhouse gases in the atmosphere was initiated through an international cooperative agreement signed in December 1997. The program is funded by agencies of the Governments of Japan, the United States, Norway, Canada, and Australia; and Asca Brown Boveri. The program consists of a series of three separate field experiments of increasing magnitude and duration. The first field experiment will be conducted in Hawaii during the summer of 2001. Quantitative data will be obtained on the dissolution and transport of pure CO₂ released at a depth of about 800 m.

To support the planning and design of the field experiment, oceanographic surveys of the site, modeling studies, and laboratory experiments are being pursued. The modeling results suggest that, at the maximum test injection rate of 1 kg/s, a plume comprising relatively large 14 mm diameter droplets will rise less than 150 m before dissolving completely. The lowest pH detected by the simulation for this case was about 6.1 (ambient pH = 7.5). Laboratory studies indicate that a wide range of CO₂ droplet sizes can be generated through appropriate design and operation of the injector. Droplet size is a principal factor that determines the extent of the affected water volume and the magnitude of induced changes to sea water chemistry. Tests also are being performed to assess the potential of hydrate blockage and to devise strategies to avoid this problem.

ACKNOWLEDGMENTS

Support by the Research Institute of Innovative Technology for the Earth (RITE) via subcontracts through the Pacific International Center for High Technology Research and the U.S. Department of Energy under Contract No. DE-FG22-95PC95206 is gratefully acknowledged. This support does not constitute an endorsement by the Department of Energy of the views expressed herein. Experiments at UH were partially supported by the Japan Industrial Technology Association (JITA).

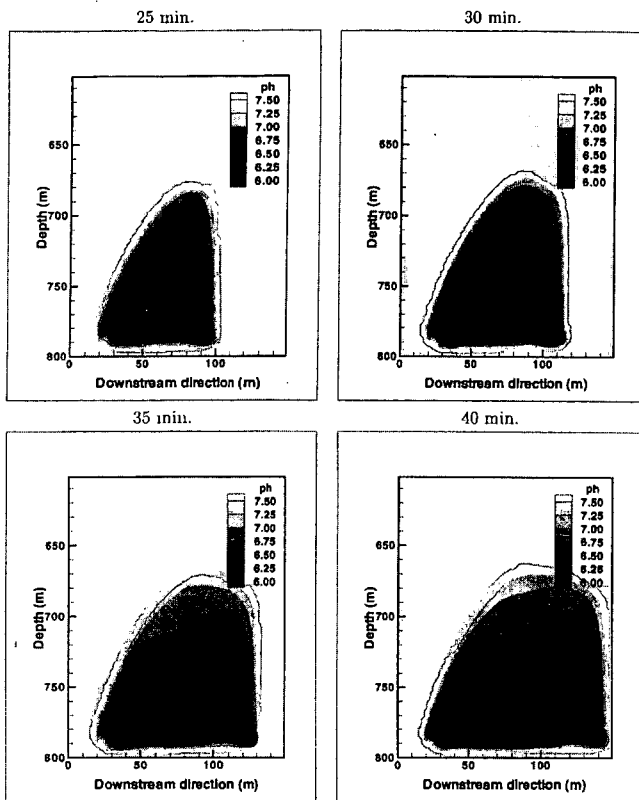


Figure 3 Supercomputer model predictions of pH distributions at different times after the start of injection; ambient pH is 7.5. 14 mm droplets of CO₂ are injected continuously at 1 kg/s at 790 m; mass transfer is assumed to be inhibited by a hydrate film.

REFERENCES

- Alendal G., H. Drange, and F. Thorkildsen, "Two-Phase Modelling of CO₂ Droplet Plumes," Technical Report No.153, NERSC, October 1998.
- Aya, I. And K. Yamane, "Stability of Clathrate-Hydrate of Carbon Dioxide in Highly Pressurized Water," *Proc. Winter Ann. Meeting of ASME*, HTD-Vol. 215, 17, 1992.
- Herzog, H, E. Drake, and E. Adams, "CO₂ Capture, Reuse and Storage Technologies for Mitigating Climate Change," White Paper prepared for U.S. Department of Energy, DE-AF22-96PC01257, 1996.
- Hirai, S., K. Okazaki, N. Araki, Y. Yazawa, H. Ito, and K. Hijikata, "Transport Phenomena of Liquid CO₂ in Pressurized Water Flow with Clathrate Hydrate at the Interface," *Energy Convers. Mgmt* 36(6-8), 471 (1995).
- Liro, C.R., E. Adams, and H. Herzog, 1992. "Modeling the Release of Carbon Dioxide in the Deep Ocean" *Energy Convers. Mgmt*. 33(5-8), 667 (1992).
- Masutani, S.M. and G.C. Nihous, "Rig Techniques and Experiments," in *IEA Greenhouse Gas R&D Programme Report on Ocean Storage of CO₂, Workshop 4-Practical and Experimental Approaches* (W. Omerod, ed.), IEA Greenhouse Gas R&D Programme, Cheltenham, UK, 1997.
- Masutani, S.M., "A Field Experiment to Investigate CO₂ Ocean Sequestration," *Proc. Deep Sea and CO₂ 2000*, 2000.
- Masutani, S.M. and G.C. Nihous, "An Update on the International Field Experiment on CO₂ Ocean Sequestration," invited paper, in *Proc. 2nd International Symposium on Ocean Sequestration of Carbon Dioxide*, 1999.
- Millero, F.J. and M.L. Sohn, *Chemical Oceanography*, CRC Press, Boca Raton, FL, 1992.
- Mori, Y., S.M. Masutani, G.C. Nihous, L.A. Vega, and C.M. Kinoshita, "Pre-combustion Removal of Carbon Dioxide from Hydrocarbon-fuelled Power Plants," *Fuel* 72(9), 1293 (1993).
- Teng, H., C.M. Kinoshita, and S.M. Masutani, "Hydrate Formation on the Surface of a CO₂ Droplet in High-Pressure/Low-Temperature Water," *Chemical Engineering Science* 50(4), 559 (1995).
- UNFCCC, Document FCCC/SBI/1997/19/Add.1, from <http://www.unfccc.de/>, 1997.
- UNFCCC, Document FCCC/CP/1997/7/Add.1, from <http://www.unfccc.de/>, 1998.

DEVELOPMENT OF A HIGH-PRESSURE WATER TUNNEL FACILITY FOR OCEAN CO₂ STORAGE EXPERIMENTATION

Robert P. Warzinski and Ronald J. Lynn
U.S. Department of Energy, National Energy Technology Laboratory
P.O. Box 10940, Pittsburgh, PA 15236-0940

Anne M. Robertson and Igor V. Haljasmaa
University of Pittsburgh, Department of Mechanical Engineering
648 Benedum Hall, Pittsburgh, PA 15260

KEYWORDS: carbon dioxide, ocean sequestration, water tunnel

INTRODUCTION

The rising atmospheric levels of greenhouse gases, primarily CO₂, due to the production and use of energy is a topic of global concern. Stabilization may require measures other than fuel switching to lower carbon energy sources, increased use of renewable energy, and improvements in efficiencies. A new way of potentially limiting atmospheric increases of CO₂ while maintaining energy diversity is carbon sequestration which entails the capture and non-atmospheric storage of the carbon emitted from energy production and use. A recent report describes the key areas of research and development presently viewed as necessary to understand the potential of carbon sequestration for managing carbon emissions (1).

One potential storage option is to directly introduce CO₂ into the ocean at depths greater than about 500 m (1,2). Part of the carbon sequestration research program at the National Energy Technology Laboratory (NETL) of the U.S. Department of Energy has involved work in this area (3,4). This work has focused primarily on the impact on this storage option of the possible formation of the icelike CO₂ clathrate hydrate (CO₂ · nH₂O; 6 < n < 8; referred to hereafter simply as hydrate) as either discrete particles or as coatings on drops of liquid CO₂. All of this prior work was performed in a small (less than 40 cm³) pressure vessel. While useful data on the formation, dissolution, and relative density of the hydrate were obtained, realistic simulation of the oceanic environment was not possible owing to contact of the species of interest with foreign (glass, stainless steel) materials in such a vessel. These foreign materials can influence hydrate formation and dissolution by acting as nucleation sites and providing unnatural heat transfer characteristics, both important factors in crystallization processes.

To attempt to overcome these limitations and provide a more realistic simulation of the deep ocean environment, a High-Pressure Water Tunnel Facility (HWTF) is being constructed that will permit experimental observations on objects such as CO₂ drops, hydrate particles or hydrate-covered CO₂ drops to be made without contact with materials other than seawater. The HWTF will permit the observation of buoyant objects in a windowed test section through the use of a countercurrent flow of water and special design features that provide for radial and axial stabilization. This paper describes the status of the experimental and theoretical efforts associated with the development of the HWTF.

DISCUSSION

In 1981, Maini and Bishnoi published work on the development of a high-pressure water tunnel to study hydrate formation on freely suspended natural gas bubbles in a simulated deep ocean environment (5). Their design considerations formed a starting point for the work at NETL on ocean sequestration of CO₂. As summarized in their paper, the hydrodynamic conditions necessary for holding an object in free suspension in such a device consist of: 1) the drag on the object should be equal to the force of buoyancy; 2) the axial velocity of the liquid should gradually increase with height to provide stability against vertical displacement; 3) the velocity distribution over a cross section of the liquid column should be axially symmetric with a local minimum at the center to provide stability against lateral displacement; and 4) the flow should be free of large-scale turbulence. To achieve the desired velocity profiles, an observation section with a tapered inner diameter and various flow conditioning devices inserted above and possibly below this section can be used.

A simplified schematic drawing of a water tunnel device is shown in Figure 1 (only inner diameters are shown). This device is placed in a flow loop that provides for recirculation of water through the system. For a positively buoyant object, the flow of water or seawater enters the top of the water tunnel and passes through a stilling section (not shown in Figure 1). At the end of the stilling section, a flow conditioning element is placed to provide the velocity profile required for radial stabilization of the buoyant object in the test section immediately below it.

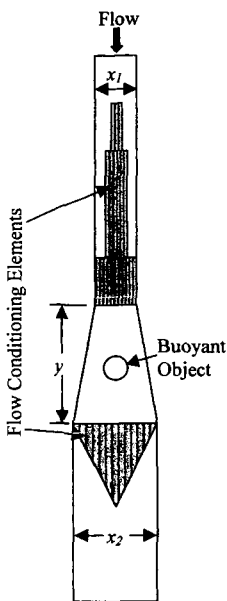


Figure 1. Schematic diagram of a water tunnel device

automatically moved across the section's diameter to obtain information related to local velocities. A computer-controlled positioning system translates the pitot tube across the test section and obtains the measurements needed to determine a velocity profile at this point in the system.

An example of velocity profile data obtained in this manner over a range of flow rates is shown in Figure 2. Only an upstream flow conditioning element similar to the top one in Figure 1 was used to create the velocity profiles shown in Figure 2.

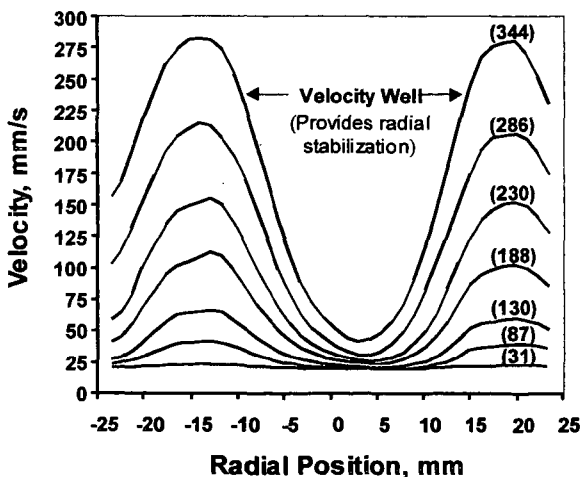


Figure 2. Velocity profiles obtained in LWTf test section using a pitot tube inserted 7.5 cm below the flow conditioning element. Each curve was obtained at a different total flow rate (average flow in cm^3/s shown in parentheses). Radial position is measured from the center of the test section.

The top flow conditioning element shown in Figure 1 represents a bundle of small tubes of different length. Various other configurations are possible. Increasing the length of the tubes in the center results in more head loss in this region and results in flow redistribution with the desired local velocity minimum in the center of the water tunnel. The diameter of the test section increases from top to bottom ($x_2 > x_1$) which provides the downstream axial velocity drop required for axial stabilization. At the exit of the test section, another flow conditioning element may be used. In Figure 1, this lower element depicts another possible tube bundle shape that could be used. A final stilling section is located after the test section (again not shown in Figure 1). Design variables affecting the velocity profile in the test section include the geometries of the conditioning elements and the divergent test section.

Both experimental and theoretical work is in progress at NETL to determine the required design parameters needed for stabilization of CO_2 in a HWTF over the range of anticipated ocean injection conditions. A Low-Pressure Water Tunnel Facility (LWTF) of similar internal dimensions ($x_1 = 5.08 \text{ cm}$, $x_2 = 6.35 \text{ cm}$) has been built to test various designs and provide information for the theoretical treatment of this problem. It consists of the water tunnel which is constructed of plexiglass pipe, a 5.08 cm ID flow loop of PVC plastic pipe, and a variable-speed centrifugal pump for water circulation. An ultrasonic flow sensing system is used to measure the total flow rate in the loop. An S-shaped pitot tube was fabricated and calibrated at NETL for insertion through ports in the test section and is

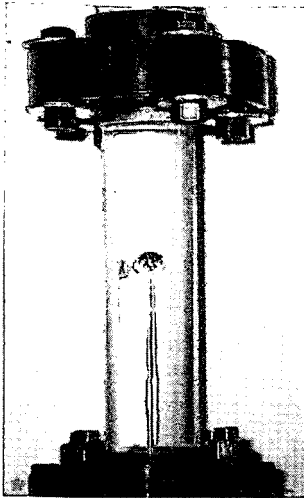


Figure 3. Air bubble stabilized in the test section of the LWTF.

Figure 3 shows an air bubble stabilized in the test section of the LWTF. Similar stability was also achieved using plastic spheres of varying size and density. A single flow conditioning element similar to the one shown in Figure 1 at the top of the test section was used. It consisted of a tube bundle containing longer tubes in the center.

In previous work (5,6), different types of flow conditioning elements were used; however no systematic analyses were performed to relate possible configurations of the flow conditioning elements to the velocity profile and the resulting positional stability of the buoyant object. Presently, in the work at NETL, theoretical optimization of flow conditioning element configuration is being pursued. This work is divided into two steps:

1. Given the mass and density of the bubble or drop (hereafter referred to as fluid particle), determine the optimal velocity profile to stabilize the position of the fluid particle;
2. Given the optimal velocity profile, find the geometry of the flow conditioning element(s) which not only produce such a profile, but also minimize

degeneration of it through the test section.

The optimum velocity profile for fluid particle stabilization is expected to vary with the regime of flow. Prior work by various researchers on bubbles and on rising and falling drops in different fluids reveals a variety of regimes, the realization of which depends on a small number of non-dimensional parameters. A non-dimensional analysis is therefore necessary to determine the relevant independent parameters for the anticipated regimes in a water tunnel device.

If a uniform flow of an incompressible fluid past the fluid particle is considered and if the effects of the wall and flow inside the fluid particle are ignored, then there are six parameters of interest, which are summarized below in Table 1.

Table 1. Parameters of Interest for Flow Analysis

Variable	Definition	Dimensions (MLT)
D_e	Effective Diameter	L
U	Free Stream Velocity	L/T
ρ_l	Liquid Density (water)	M/L^3
$\Delta\rho$	Density Differential ($\rho_l - \rho_b$)	M/L^3
μ_l	Viscosity of Liquid	$M/(LT)$
γ	Surface Tension	M/T^2

There are three primary dimensions for the six physical and geometric parameters: mass, length, and time (MLT). From the Buckingham Pi Theorem, it follows that there will be three independent dimensionless numbers for this system. The choice of these dimensionless parameters is not unique, which means there is some freedom to choose parameters which are the most suitable for this analysis.

It is helpful to relate the definitions of the dimensionless numbers to characteristic values of the effective forces acting on the fluid particle. Four considered effective forces are shown below in Table 2.

Table 2. Effective Forces Acting on a Fluid Particle

Effective Forces	Characteristic Magnitudes
Viscous Forces	$\mu_l U D_e$
Buoyancy Forces	$\Delta\rho g D_e^3$
Surface Tension Forces	γD_e
Inertial Effects	$\rho_l U^2 D_e^2$

Displayed in Table 3 are the definitions of commonly used dimensionless numbers for bubbles in uniform flow. Various triplets of these dimensionless numbers are used in the literature (7,8):

Table 3. Dimensionless Variables for Flow Analysis

Non-dim. Variable	Name	Ratio of Physical Phenomena	Definition
Re	Reynolds Number	Inertial/viscous	$\rho_l U D_c / \mu_l$
Ca	Capillary Number	Viscous/surface tension	$\mu_l U / \gamma$
Eo	Eotvos Number	Buoyancy/surface tension	$(\Delta \rho g D_c^2) / \gamma$
We	Weber Number	Inertial/surface tension	$(\rho_l U^2 D_c) / \gamma$
Wg	Inertial Buoyancy Parameter	Inertial/buoyancy	$(\rho_l U^2) / (\Delta \rho g D_c)$
Cg	Viscous Buoyancy Parameter	Viscous/buoyancy	$(\mu_l U) / (\Delta \rho g D_c^2)$
Mo	Morton Number		$(\Delta \rho g \mu_l^4) / (\rho_l \gamma^3)$

Reference 7 considers shape regimes for fluid particles as a function of Re and Eo numbers. There exist two limiting cases where the analysis can be significantly simplified:

Case 1. Small Re and Eo numbers, under which the fluid particle has an almost spherical shape. Often, this regime is realized for very small particles (<0.5mm in diameter), or for the slow motion of the fluid particle caused by a very small buoyant force (small difference in density). In this case the terminal velocity of the fluid particle can be expressed (9,10) as:

$$U_{term} = \frac{1}{K} \frac{D_c^2 g \Delta \rho}{\mu_l} \quad (1)$$

(constant K spans from 12 to 36 in different theories and is believed to depend on surface active impurities in the liquid).

Case 2. Large Re and Eo numbers, under which the fluid particle has a spherical cap shape with a well determined front boundary and an unstable, wavy rear boundary caused by the wake behind the fluid particle. Often, this regime is realized for large bubbles (> 2 cm³ volume), when inertial effects dominate viscous effects and surface tension. Then, the terminal velocity of the fluid particle can be expressed (7) as:

$$U_{term} = \frac{2}{3} \sqrt[3]{gR \frac{\Delta \rho}{\rho_l}} \quad (2)$$

where R is radius of curvature of the fluid particle at the stagnation point.

For intermediate values of Re and Eo, different kinds of transitional regimes occur which are essentially unstable. Therefore, it would be beneficial to design experiments corresponding to one of the limiting cases outlined above.

The liquid CO₂ particle/seawater system is expected to exhibit Case 1 behavior since the densities of seawater and CO₂ are not that different under anticipated direct ocean injection conditions. Owing to its greater compressibility, at depths greater than about 2700 m, liquid CO₂ can even be more dense than seawater. Sphericity of the fluid particle can significantly simplify both the theoretical analysis and experimental observations. Past experimental works show that for a small Re number, fluid particles of almost spherical shape exhibit a rectilinear motion. As the Reynolds number is increased, the wake behind the particle begins to oscillate and further increases in Reynolds number lead to periodic shedding of the vortices (9). Absence of lateral oscillations and significant wakes behind the fluid particle at low Reynolds numbers makes this regime very attractive for initial experiments involving hydrate formation. Hence, it would be useful to determine the optimum size of the fluid particle, small enough to be in the spherical regime, but big enough for meaningful observations. Preliminary non-dimensional analysis shows that at the depths of about 2400-3000 m, a CO₂ fluid particle of 1-cm diameter should be close to spherical. When the optimum size of the fluid particle is determined, optimum flow conditioning elements for this particular size can be developed.

The HWTF has been designed to permit investigation of other species, such as other flue gas components (N₂, O₂, SO₂) and natural gas components, which may have properties quite

different than those of CO₂. In these cases, behavior more like Case 2 may be encountered. The modeling work will eventually be extended to develop flow conditioning elements for such systems.

In conjunction with the measurements being made using the LWTF, a preliminary simplified analytical evaluation of the flow conditioning system used in LWTF has been completed. This evaluation provides an approximation for the velocity distribution immediately downstream of the flow conditioner due to different resistances across the tube bundle system. Having a data base of different profiles corresponding to different flow conditioners will permit the appropriate design of the flow conditioner to be selected to meet the desirable velocity profile for fluid particle stabilization. It will then be used to guide the design of the flow conditioning elements for the HWTF.

In order to avoid the assumptions inherent in the simplified analytical evaluation, full three-dimensional finite element analysis (FEA) of the flow through the conditioning element will be performed. This numerical approach enables both a more accurate model of the actual element geometry and the exploration of the velocity profile degeneration downstream of the conditioning element.

The numerical domain will include a straight section upstream of the spoiler, the spoiler system, and the diverging/converging test section downstream of the spoiler. The straight upstream section is included since the velocity profile immediately upstream of the flow conditioning element is not known a priori. This length of the upstream section is made long enough to approximate fully developed inlet conditions. If necessary, the actual inlet geometry of the experimental device can be included. From this three dimensional analysis, velocity profiles throughout the test chamber can be obtained.

The theoretical analyses described above is a sizeable analytical and numerical challenge. This work is not only necessary for the design optimization of the flow conditioning elements and internal geometry of the HWTF for CO₂ ocean sequestration research, but will also be useful in utilizing the device in applications involving different fluids.

ACKNOWLEDGEMENTS

The authors wish to thank Jerry Foster and Jay Levander for their assistance in developing the LWTF.

REFERENCES

1. *Carbon Sequestration Research and Development*, U.S. Department of Energy Report, DOE/SC/FE-1, 1999, available NTIS.
2. Herzog, H. *Greenhouse Gas Control Technologies*, B. Eliasson, P.W.F. Riemer, and A. Wokaun, eds., Pergamon, Amsterdam, 1999, 237-242.
3. Warzinski, R.P., G.D. Holder *Ibid*, 1061-1063.
4. Warzinski, R.P., R. J. Lynn, G.D. Holder *Third International Conference on Gas Hydrates, Annals of the New York Academy of Sciences*, in press, 1999.
5. Maini, B.B. & P.R. Bishnoi *Chem. Engng. Science* 36, 1981, 183-189.
6. Moo-Young, M., G. Fulford, I. Cheyne. *Ind. Eng. Chem. Fundam.*, 10(1), 1971, 157-160.
7. Clift, R., J. R. Grace, M. E. Weber. *Bubbles, Drops, and Particles*, Academic Press, 1978.
8. Leal, L.G. *Computational Studies of Drop and Bubble Dynamics in a Viscous Fluid*, Drops and Bubbles, Third International Colloquium, 1988, 147-168.
9. Batchelor, G.K. *An Introduction to Fluid Dynamics*, Cambridge Univ. Press, 1967.
10. L.-S. Fan, K. Tsuchiya, *Bubble wake Dynamics in Liquids and Liquid-Solid Suspensions* (Butterworth - Heinemann), 1990.

**CHARACTERISTICS AND PERFORMANCE
OF A DEEP OCEAN DISPOSAL SYSTEM
FOR LOW-PURITY CO₂ GAS BY GAS LIFT EFFECT**

Takayuki Saito
National Institute for Resources and Environment
Onogawa 16-3, Tsukuba
Ibaraki 305-8569, Japan
(Permanent address: Shizuoka University
3-5-1 Johoku, Hamamatsu
Shizuoka 432-8561, Japan)

Sanai Kosugi
Sumitomo Metal Industries Ltd.
8-2, Honshio-cho, Shinjuku-ku
Tokyo 160-0003, Japan

Takeo Kajishima
Osaka University
2-1 Yamadaoka, Suita
Osaka 565-0871, Japan

Katsumi Tsuchiya
Tokushima University
Minamijosanjima-cho, Tokushima
Tokushima 770-0814, Japan

KEYWORDS: Gas lift effect, Ocean disposal, Carbon dioxide

ABSTRACT

Progressive Gas Lift Advanced Dissolution (P-GLAD) system has been newly developed to mitigate the global warming. The system dissolves low-purity CO₂ gas in seawater at shallow portions and sequesters CO₂ at the deep ocean. The system is an inverse-J pipeline set in the ocean between 200 and 3000m in depth. Usual methods of deep-sea sequestration such as storage of liquid CO₂ at the deep-sea floor and deep-sea releasing of liquid CO₂ consume huge amount of energy, because these need high-purity capture and liquefaction of CO₂. To realize deep-sea sequestration with low energy consumption and low environmental impact, we utilize a gas-lift effect to dissolve low-purity CO₂ into seawater and transport CO₂ solution to a great depth. The present paper describes basic characteristics and performance of the system for low-purity CO₂ gases. We also discuss cost estimate including a system for capture of CO₂ gas and construction of P-GLAD.

INTRODUCTION

The global warming mainly due to the increase of atmospheric CO₂ concentration is getting serious. A countermeasure that can economically and effectively treat huge amount of CO₂ (23GtC/year) emitted by human activities should be developed. Ocean sequestration of CO₂ is a hopeful option to mitigate the increase in the atmospheric CO₂ concentration, because the ocean has been absorbing and sequestering CO₂ through the history of the earth, and the absorption capacity is enormous [Hoffert, 1979]. Several ideas of ocean disposal of CO₂ have been proposed. They are categorized as follows: a) storage of liquid CO₂ on the deep-sea floor deeper than about 3000m, in the idea CO₂ is stored on the deep sea flow as CO₂ ponds covered with CO₂ gas hydrate [Ohsumi, 1993]; b) direct release of liquid CO₂ into the intermediate depth water of 1000-3000m [Liro, 1992]; c) direct release of gaseous CO₂ into shallow water and use of gravity current [Haugan, 1992], the idea is direct release of gaseous CO₂ into the seawater at a depth of 200-400m and expecting sink of CO₂-rich seawater to the deep-sea by the density difference between the solution and ambient seawater.

Long term isolation, more than several hundreds years, of CO₂ from the atmosphere is expected in the methods a) and b), because the initial injection point is in intermediate or deep water. Though deeper initial injection assures longer-term isolation, these two methods need high-purity capture and separation, and liquefaction of CO₂. Higher-purity separation of CO₂ from exhausted gas consumes larger energy. They inevitably consume huge amount of extra energy in these preprocessing. The deep initial injection brings the deep ocean secondary environmental impact, namely acidity by dense CO₂ solution. Since the method c) need no liquefaction, it improves an amount of energy consumption. Density and/or temperature layers in the ocean, which grow in middle and low latitude area, prevent sinking of CO₂ solution to a great depth. In this case, long-term isolation is no longer expected.

A method of the ocean sequestration has to isolate huge amount of CO₂ from the atmosphere for long term, several hundreds or thousand years, with low cost, low energy consumption and low environmental impact. To realize this, the preprocessing should be low-purity separation and no

liquefaction; besides the disposal method should be able to deal with low-purity CO₂ gas. We have been improving GLAD system, which is an ocean sequestration system for pure CO₂ gas using gas lift effect [Saito, 1996; Saito 1997; Saito, 2000; Kajishima, 1995; Kajishima, 1997]. We have developed P-GLAD (Progressive Gas Lift Advanced Dissolution, See Fig.1) system [Saito, 1999a, b] for low-purity CO₂ gas. In the present paper, we discuss performance, cost estimate and environmental receptivity of P-GLAD by experimental and numerical simulation. First, we describe experimental results on solubility and pumping performance of the system. Second, essence of numerical method is explained. Agreement of numerical results with experimental ones is discussed. Third, acidity of the solution released from the system is discussed. Finally, based on these discussions cost estimate for P-GLAD and comparison of the cost with usual method are performed.

EXPERIMENT

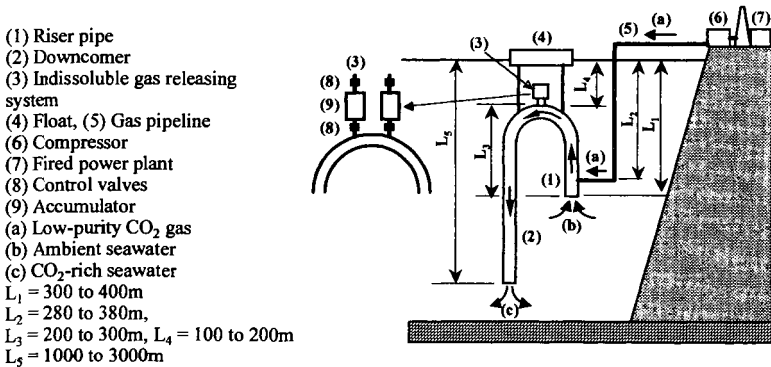
Experimental setup used in the present investigation, a laboratory-scale P-GLAD system, is illustrated in Fig. 2. The riser pipe (1) and the downcomer (2) are made of acrylic transparent pipes of 25mm in diameter and 7.69m in height. The riser is connected to two pressure vessels (4) made of stainless pipe of 106.3mm in diameter and 8.19m in height. The downcomer is placed inside the vessel. The top of the riser is equipped with an indissoluble gas-releasing device (3), which releases indissoluble gases of N₂ and O₂. Low-purity CO₂ gas, mixture of pure CO₂ gas (99.9% purity) and pure air (CO<1ppm, CO₂<1ppm and CH₄<1ppm) well mixed in a gas-mixing accumulator (10), is injected into the riser through a gas injector (5). The gas-injector has an annular structure; the inner pipe of acrylic resin with 25mm in diameter is equipped with 108 small capillaries of 0.78mm in diameter; outer pipe is made of stainless steel of 106.3mm in diameter.

Tap water is supplied at the top of each pressure vessel after filtration by a 1μm filter. Our experiments were performed under overflowing condition. The temperatures of the supplied water and the gas-liquid mixtures were between 287 and 290K.

MESUREMENT

Superficial velocity of the liquid phase J_L was measured using an electromagnetic flowmeter (A), the temperature and static pressure in the riser using thermo couples (B) and pressure transducers (C), respectively. We measured and controlled mass flow rate of each gas, Q_{CO_2} and Q_{AIR} using mass flow controllers (E) and (F).

Performance of solubility of the laboratory-scale P-GLAD is calculated from CO₂ molar concentration of the gas phase in the riser [Saito, 1999a]. First, we visualized and recorded the bubbly flows in the riser using two sets of high-speed video systems of 500 frames/s and stroboscopes of 10μs of flashing rate (C). Second, we analyzed the images by digital image processing. Third, bubble characteristics such as volume, surface area, location and velocity were calculated from the processing results. Finally, the molar concentration and solubility were calculated from the above characterization of bubbles.



The main part of the P-GLAD system is an inverse-J pipeline (1) and (2), and an indissoluble gas releasing system (3). The low-purity CO₂ gas (a) is injected into the riser pipe (1) at a depth between 200 and 400m. An upward current occurs in the pipe by a gas-lift effect. CO₂ included in the bubbles dissolves into seawater while the bubbles rise in the riser. Ambient seawater (b) is flowing at the bottom of the riser. Indissoluble gas of N₂ is released at the top of the riser by an indissoluble gas releasing system (3). The downcomer (2) is used as a transportation pass of the CO₂-rich seawater (c) to a great depth between 1000 and 3000m. An additional downward current is generated in the downcomer owing to the density difference between the CO₂-rich and ambient seawater. Thus, the bubble dissolution and the transportation of CO₂-rich seawater to great depths are enhanced in the P-GLAD system by the gas lift effect.

Fig.1 Concept and principle of the P-GLAD system

- (1) Dissolution pipe
 - (2) Drainpipe
 - (3) Indissoluble gas releasing device
 - (4) Pressure vessels
 - (5) Gas injector
 - (6) Observing windows
 - (7) Camera lifter
 - (8) CO₂-gas cylinder
 - (9) Pure-air cylinder
 - (10) Gas mixing accumulator
- (A) Electromagnetic flowmeter
 - (B) Thermo couplers
 - (C) Pressure transducers
 - (D) High-speed video systems & strobes
 - (E) & (F) Mass flow controller

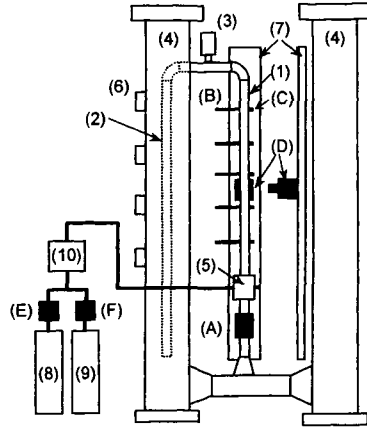


Fig. 2 Experimental setup

NUMERICAL SIMULATION

The Lagrange method was applied for the each bubbles, and the Euler method for the liquid phase. Conservation laws of mass and momentum for each phase were employed. Trapp & Mortensen scheme was used in our computation [Trapp, 1993]. In the present investigation, applying the Lagrange method mass conservation law of dispersed gas phase is expressed as following equation.

$$\frac{d}{dt}(\rho_p V_p) = -k_L M_p (C_s - C) A_p \quad (1)$$

where k_L represents the mass transfer coefficient, $V_p (= 4\pi r_p^3/3)$ the bubble volume, $A_p (= 4\pi r_p^2)$ the surface area, and r_p the equivalent diameter of bubble. Density of gas phase ρ_p is calculated from the ideal gas equation. C_s is the molar concentration of CO₂ on the bubble surface and defined as saturated concentration of CO₂ calculated from Henry's law. C is the molar concentration of CO₂ in the solution, estimated by the equation of convective diffusion.

$$\frac{dC}{dt} + J_1 \frac{dC}{dx} = D_1 \frac{d^2 C}{dx^2} + q_s \quad (2)$$

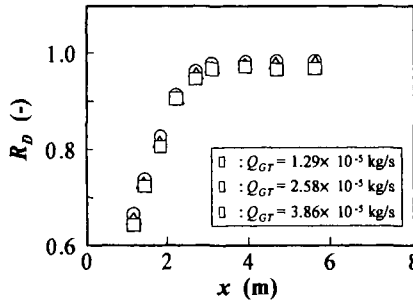


Fig. 3 Axial profiles of dissolution ratio in the riser. $Q_{GR} = Q_{CO_2} + Q_{AIR}$

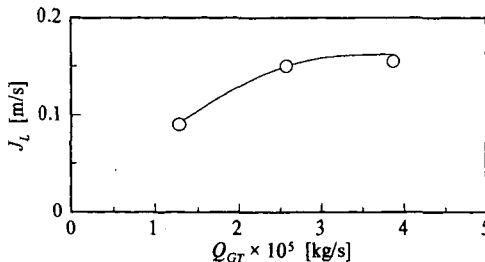


Fig. 4 Superficial velocity of liquid phase in the riser as a function of gas injection rate.

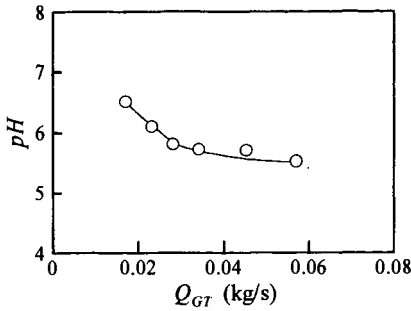


Fig. 5 Acidity of CO₂ solution discharged from the laboratory P-GLAD.

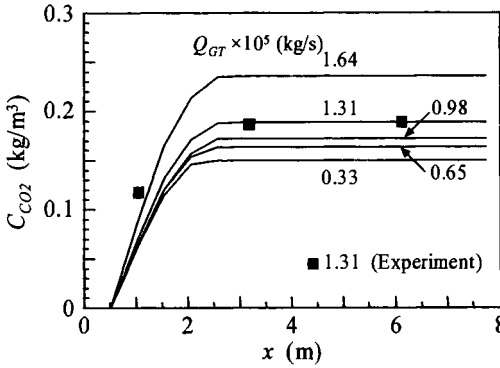


Fig. 6 Computational results on CO₂ concentration in solution compared with experimental ones.

q_g represents the rate of dissolution, $J_L [(1 - \alpha)u_l]$ the superficial velocity of liquid phase, α the void fraction, u_l the velocity of liquid phase. D_T is the turbulent diffusion coefficient calculated from liquid phase flow of Reynolds number $J_L D/\nu$ using $k-\varepsilon$ model, where ν is kinematic viscosity.

EXPERIMENTAL AND COMPUTATIONAL RESULTS

Defining CO₂ gas dissolution ratio as $R_D = Q_{CO_2, dis}/Q_{CO_2}$, the axial profile is plotted in Fig. 3, where $Q_{CO_2, dis}$ represents the mass of CO₂ dissolved in liquid phase, and Q_{CO_2} the mass of CO₂ included in injected gas. R_D rapidly increases for $z < 3$ m, and most of the CO₂ gas injected dissolves into the water phase in the section. The maximum values of R_D are 0.979, 0.955 and 0.964. P-GLAD shows satisfactory performance of CO₂ gas dissolution.

Superficial velocity of liquid phase J_L , namely lifted water velocity, is shown in Fig. 4 as a function of gas injection rate Q_{GT} . J_L gradually increases with increase in Q_{GT} before 3×10^{-5} kg/s. After the value, J_L is almost saturated. In higher gas injection rate, it was observed that indissoluble gas remained at the top of the riser. As a result, saturation of J_L occurs owing to increase in friction loss there.

Acidity of CO₂ solution discharged from laboratory-scale P-GLAD is plotted in Fig. 5 as a function of gas injection rate. The acidity increases with increase in gas injection rate. The value of pH is in the range between 5.5 and 6.5 in the present investigation. The acidity is moderate. Besides the acidity is controllable by adjusting the gas injection rate.

Figure 6 shows computational results on CO₂ concentration in solution and comparison of them with those of the experiment. Computational results show a good agreement with the experimental ones. Therefore, our numerical modeling and computational scheme is reasonable.

COST ESTIMATE

Before cost estimate, we carried out experiments using a large-diameter-pipe loop (150mm in diameter). Large-scale structure and turbulence mechanism of bubbly flows in a large diameter pipe were obtained [Mudde & Saito, 2000]. We performed cost estimate of P-GLAD for 1,000MW fired power plant listed in Table 1 on the basis of above experimental and numerical results. Gas transportation plant, CO₂ capture and separation plant, and dimension of P-GLAD

Table 1 Dimension of fired power plant.

Generating capacity	1,000MW
Location	Seaside
Rate of CO ₂ discharge	100kg/s (360ton/s)

Table 2 Gas transportation plant.

Compressor power	40,000kw
Compressor location	Power plant site
Length of pipeline	100km
Diameter of pipe	0.5m
Material of pipe	High-tension steel

Table 3 CO₂ capture and separation plant.

Method	PSA (1 stage)
Adsorption	Under atmospheric pressure
Degassing	Under vacuumed
Dewatering tower	φ12.5m×H36m×16units
Number of adsorption/degassing tower	φ6m×L40m×16units
Adsorption material for CO ₂	Zeorite
Adsorption material for water	Activated aluminum + Zeorite

Table 4 Dimension of P-GLAD.

Riser	φ0.5m×H300m×90units, High-tension steel
Downcomer	φ0.5m×L10km×90units, Rain-forced FEP steel
Gas injection depth	200m
Releasing depth	1000m
Float	φ11.6m×W150m
Anchoring	Tension leg

Table 5 Cost estimate of P-GLAD and comparison of the cost with that of a usual method (direct release of liquid CO₂).

	P-GLAD (US\$/ton-CO ₂)	Usual (US\$/ton-CO ₂)
Capture & separation	26	43
Liquefaction	0	64
Transportation	30	7
Sequestration	12	12
Total	68	126

are listed in Table 2 to Table 4, respectively. We estimated a total cost of the ocean sequestration by P-GLAD considering construction, operation, labor cost (in Japan), land cost (in Japan), tax (in Japan), interest and a price reduction. The result is summarized in Table 5. Total cost of P-GLAD is a half of that of a usual method. Economical feasibility of P-GLAD is very higher than that of a usual method such as direct release of liquid CO₂ into intermediate depth water.

CONCLUSION

We discussed performance and characteristics of P-GLAD (Progressive Gas Lift Advanced Dissolution system) experimentally and numerically. We obtained P-GLAD has satisfactory performance as an ocean sequestration system of low-purity CO₂ gas. On the basis of these results, we performed cost estimate of a total system of P-GLAD. P-GLAD showed highly economical feasibility.

REFERENCE

- Haugan, P. M. & Drange, H., *Nature*, Vol. 357, 318, (1992).
 Hoffert, M. I., Wey, Y. C., Callegari A. J. & Broecker, W. S., (1997), *Climatic Change*, Vol. 1, 59.
 Kajishima, T. Saito, T. and Nagaosa, R., (1995), *Energy Conve. and Manag.*, Vol. 36, 467.
 Kajishima, T. Saito, T. and Nagaosa, R., (1997), *Energy*, Vol. 22, 257.
 Liro, C. R., Adams, E. E. & Herzog, H. J., (1992), *Energy Conve. and Manag.*, Vol. 33, 667.
 Mudde, R. F. and Saito, T., submitted to *J. of Fluid Mech.*, (2000)
 Ohsumi, T., *Energy Conversion and Management*, Vol. 34, 1059, (1993).
 Saito, T., Kajishima, T., Tsuchiya, K. and Kosugi, S., (1999a) *Chem. Eng. Sci.*, Vol. 54, 4945.
 Saito, T., Kajishima, T., and Tsuchiya, K., (1999b), applied to EU, US and Australian patent.
 Saito, T. and Kajishima, T., (1996), *ACS, Division of Fuel Chemistry*, Vol. 41, 1441.
 Saito, T. and Kajishima, T., (1997), US patent, No. 5662837.
 Saito, T., Kajishima, T. and Nagaosa, R., (2000), reviewed in *ES & T*.
 Trapp, J. A. and Mortensen, G. A., *J. of Comput. Phys.*, Vol. 107, 367, (1993)